

## Mixing of polar vortex air into middle latitudes as revealed by tracer-tracer scatterplots

D. W. Waugh,<sup>1</sup> R. A. Plumb,<sup>2</sup> J. W. Elkins,<sup>3</sup> D. W. Fahey,<sup>4</sup> K. A. Boering,<sup>5</sup> G. S. Dutton,<sup>3,6</sup> C. M. Volk,<sup>3,6</sup> E. Keim,<sup>4,6</sup> R.-S. Gao,<sup>6</sup> B.C. Daube,<sup>5</sup> S. C. Wofsy,<sup>5</sup> M. Loewenstein,<sup>7</sup> J. R. Podolske,<sup>7</sup> K. R. Chan,<sup>7</sup> M. H. Proffitt,<sup>4,6</sup> K. K. Kelly,<sup>4</sup> P. A. Newman,<sup>8</sup> and L. R. Lait<sup>8</sup>

**Abstract.** The occurrence of mixing of polar vortex air with midlatitude air is investigated by examining the scatterplots of insitu measurements of long-lived tracers from the NASA ER-2 aircraft during the Stratospheric Photochemistry, Aerosols and Dynamics Expedition (SPADE, April, May 1993; northern hemisphere) and the Airborne Southern Hemisphere Ozone Experiment / Measurements for Assessing the Effects of Stratospheric Aircraft (ASHOE/MAESA, March-October 1994; southern hemisphere) campaigns. The tracer-tracer scatterplots from SPADE form correlation curves which differ from those measured during previous aircraft campaigns (Airborne Antarctic Ozone Experiment (AAOE), Airborne Arctic Stratospheric Experiments I (AASE I) and II (AASE II)). It is argued that these anomalous linear correlation curves are “mixing lines” resulting from the recent mixing of polar vortex air into the middle latitude environment. Further support for this mixing scenario is provided by contour advection calculations and calculations with a simple one-dimensional strain-diffusion model. The scatterplots from the midwinter deployments of ASHOE/MAESA are consistent with those from previous midwinter measurements (i.e., no mixing lines), but the spring CO<sub>2</sub>:N<sub>2</sub>O scatterplots form altitude-dependent mixing lines which indicate that air from the vortex edge region (but not from the inner vortex) is mixing with midlatitude air during this period. These results suggest that at altitudes above about 16 km the mixing of polar vortex air into middle latitudes varies with season: in northern and southern midwinter this mixing rarely occurs, in southern spring mixing of vortex-edge air occurs, and after the vortex breakup mixing of inner vortex air occurs.

### 1. Introduction

The extent of mixing of polar vortex and midlatitude air is important for understanding the underlying cause of ozone depletion observed in middle latitudes. In recent years a controversial issue has been whether the

polar vortices act as “containment vessels” or “flow reactors” [e.g., *Randel*, 1993]. There is now substantial evidence from observational and modeling studies that above about 16 km air deep inside the polar vortex is essentially isolated from extravortical air, but that air in the vortex edge region (the region of strong horizontal gradients in long-lived tracers and potential vorticity) is sporadically transported to middle and low latitudes. Below 16 km, there appears to be more exchange between the polar vortices and middle latitudes. However, there remain uncertainties in the rate of this transport/mixing and its effect on middle latitudes, due at least partly to the lack of data available at these levels. See *World Meteorological Organization (WMO)* [1995], and references therein, for detailed discussion of the above issues.

In this paper, we investigate the extent to which polar vortex air is mixed with midlatitude air by examining the tracer-tracer scatter plots for measurements of long-lived tracers made during NASA ER-2 aircraft campaigns: the Airborne Antarctic Ozone Experiment (AAOE), the Airborne Arctic Stratospheric Experiments (AASE I and II), the Stratospheric Photo-

<sup>1</sup>Cooperative Research Centre for Southern Hemisphere Meteorology, Monash University, Clayton, Victoria, Australia

<sup>2</sup>Department of Earth, Atmosphere and Planetary Sciences, Massachusetts Institute of Technology, Cambridge, Massachusetts

<sup>3</sup>NOAA Climate Monitoring and Diagnostics Laboratory, Boulder, Colorado

<sup>4</sup>NOAA Aeronomy Laboratory, Boulder, Colorado

<sup>5</sup>Department of Earth and Planetary Science, Harvard University, Massachusetts

<sup>6</sup>Cooperative Institute for Research in Environmental Sciences, Boulder, Colorado

<sup>7</sup>NASA Ames Research Center, Moffett Field, California

<sup>8</sup>NASA Goddard Space Flight Center, Greenbelt, Maryland

chemistry, Aerosols and Dynamics Expedition (SPADE), and the Airborne Southern Hemisphere Ozone Experiment / Measurements for Assessing the Effects of Stratospheric Aircraft (ASHOE/MAESA) campaigns. In particular, we examine the anomalous behavior of interrelationships between long-lived tracers which deviate from relationships derived from earlier aircraft campaigns and from two-dimensional chemical transport models. We argue that these anomalous relationships are produced by the mixing of air from within and from the edge of the polar vortex with midlatitude air.

The interrelationships between the mixing ratios of long-lived tracers from the above aircraft campaigns have been used previously to identify anomalous chemistry (such as ozone destruction and denitrification), to determine fluxes into the troposphere, and to characterize and quantify transport into and within the lower stratosphere [e.g., Proffitt *et al.*, 1989a,b, 1990, 1993; Kelly *et al.*, 1989; Fahey *et al.*, 1989, 1990b; Murphy and Fahey, 1994; Tuck *et al.*, 1994; Boering *et al.* 1994, 1995; Wofsy *et al.*, 1994b; Volk *et al.* 1996]. In the majority of these studies the analysis was based on the fact that the points on scatterplots of long-lived tracers usually form smoothly varying curves (so-called “compact” correlation curves). Plumb and Ko [1992] argued that these correlation curves are expected if the tracers are in “slope equilibrium”, i.e., if quasi-horizontal mixing along isentropes is much faster than the residual advection (which ensures that isentropic gradients are weak) and if both are much faster than chemical processes. However, the existence of a compact correlation in a localized region does not necessarily imply slope equilibrium. During winter, for example, the requirements for slope equilibrium are generally not satisfied at the vortex edge region: the tracer isopleths are not “almost parallel” to the mixing surfaces (isentropes) in this region because quasi-horizontal mixing is not significantly faster than vertical advection. If the vortex is totally isolated, then long-lived tracers will retain compact correlations (see section 6 of Plumb and Ko [1992]), but if air is mixed across the vortex edge the compact correlation may break down.

To see this, consider the effect of mixing two air-masses on tracer-tracer scatterplots. The solid curve in Figure 1 represents the typical or “standard” correlation curve of two long-lived tracers. An air-mass with uniform mixing ratios of tracers appears on a tracer-tracer scatterplot as a single point. If two such air-masses are incompletely mixed together, the resultant air-mass has a range of mixing ratios which appear on a scatterplot as a line of points lying between the two points corresponding to the original air-masses, e.g., the dashed lines in Figure 1. As the mixing proceeds, the mixing ratios within the new air-mass become uniform, and the line of points on the scatterplot collapses to a single point corresponding to the mass-weighted average of the mixing ratios of the two original air-masses, denoted by the triangle in Figure 1. This mixing does

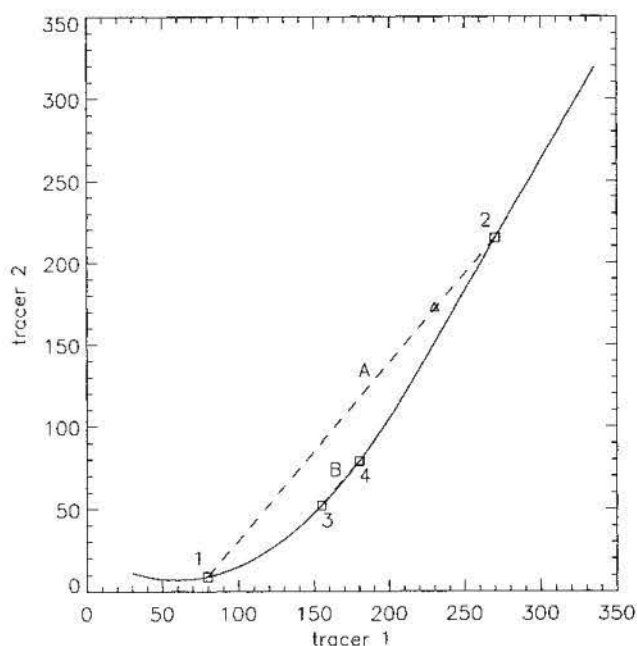


**Figure 1.** Schematic diagram of the effect of mixing on tracer-tracer scatter plots. The solid curve represents the “standard” correlation curve of two long-lived tracers. The triangle represents the result of total mixing between the discrete air-masses labelled 1 and 2 (note that this represents the case where the mass of air-mass 2 is larger than that of air-mass 1). Partial mixing between the discrete air-masses labeled 1 and 2 produces an anomalous mixing line (dashed line A), but mixing of the discrete air-masses labeled 3 and 4 (dashed line B) does not significantly alter the scatterplot.

not produce an anomalous mixing line if the standard correlation is linear in the region affected by the mixing (e.g., mixing of the discrete air-masses labeled 3 and 4 in Figure 1). However, if the tracer-tracer correlation is curved, the mixing produces an anomalous mixing line, as indicated by the dashed line A in Figure 1. Scatterplots of conserved variables, and the occurrence of mixing lines, have been used in this way to examine mixing processes within clouds [e.g., Emanuel, 1994, and references therein].

The mixing line A is anomalous in the sense that it represents a departure from “standard” tracer-tracer relationships and, as such, must be indicative of anomalous transport processes. Within the midlatitude surf zones, vigorous mixing is occurring most of the time. However, under the assumptions of Plumb and Ko [1992], isentropic gradients are weak, and so isentropic mixing will only mix air-masses with similar tracer mixing ratios. Thus isentropic mixing is occurring locally between close points on tracer-tracer scatter plots, and a single such event would thus produce a mixing line only marginally off the standard curve (see dashed line B in Figure 1). Continuous mixing would thus lead to a slow evolution of the correlation curve, without significantly destroying its compactness, or, in steady state, its ef-

facts could be balanced by slow sources and sinks. Mixing of the kind that can produce lines like A in Figure 1 must therefore be anomalous, occurring where mixing is not usually dominant and thus where the assumptions of slope equilibrium are not satisfied.

As noted above, curvature in the tracer-tracer relationship is necessary to render the effects of mixing visible. Among the tracers nitrous oxide ( $\text{N}_2\text{O}$ ), chlorofluorocarbon-11 (CFC-11,  $\text{CCl}_3\text{F}$ ), total reactive nitrogen ( $\text{NO}_y$ ), and carbon dioxide ( $\text{CO}_2$ ), different pairs of species yield relationships of different shapes; those relationships that exhibit curvature do so in regions in tracer-tracer space that correspond to different regions in physical space. For example, at altitudes sampled by the ER-2, the scatterplots of CFC-11 and  $\text{NO}_y$  against  $\text{N}_2\text{O}$  form correlation curves that are almost linear outside the vortex but curved just inside the vortex, while the  $\text{CO}_2$  versus  $\text{N}_2\text{O}$  relationship curves at and just outside the vortex edge. Thus, these relationships will display anomalous behavior only in response to mixing across the vortex edge (for CFC-11 and  $\text{NO}_y$  versus  $\text{N}_2\text{O}$ ) or between the edge and middle latitudes (for  $\text{CO}_2$  versus  $\text{N}_2\text{O}$ ). In what follows, we show how these different windows may be exploited to reveal stratospheric mixing processes and their effects on tracers.

Anomalous "mixing lines" are indeed seen in the scatterplots of long-lived tracers measured during SPADE and ASHOE/MAESA. In the next section we examine the data from the SPADE campaign. The anomalous correlation curves are shown to be consistent with the mixing of polar vortex and middle latitude air. The evolution of the polar vortex during the 1992/1993 northern winter and, in particular, the mixing of vortex and middle latitude air is examined in Section 3. Contour advection calculations indicate that during SPADE the fragments of the vortex were stretched into thin, sloping sheets, and the locations of these sheets agree well with where the anomalous data were measured. In section 4, a one-dimensional strain-diffusion model is used to examine different mixing scenarios. We show how this mixing is manifested in the tracer-tracer scatterplots and estimate the rate at which vortex air is mixed with middle latitude air in northern hemisphere spring. Scatterplots of  $\text{CO}_2$ , CFC-11, and  $\text{NO}_y$  versus  $\text{N}_2\text{O}$  from ASHOE/MAESA are discussed in section 5, with emphasis on the  $\text{CO}_2$ : $\text{N}_2\text{O}$  scatterplots from October 1994 which form mixing lines that are potential temperature dependent. Because no mixing of inner vortex air with midlatitude air is evident in the CFC-11: $\text{N}_2\text{O}$  and  $\text{NO}_y$ : $\text{N}_2\text{O}$  relationships, we argue that the straight lines in the  $\text{CO}_2$ : $\text{N}_2\text{O}$  scatterplots are produced by mixing of air into middle latitudes from the vortex edge region but not from the inner vortex. Concluding remarks are in the final section.

## 2. SPADE Measurements

### 2.1. Data

In situ measurements of a large range of chemical species were made aboard the NASA ER-2 aircraft from  $15^\circ\text{N}$  to  $60^\circ\text{N}$  during SPADE in November 1992, and April, May, and October 1993 [Wofsy *et al.*, 1994a]. In this section we examine the measurements of the chemical tracers  $\text{N}_2\text{O}$ , CFC-11,  $\text{CCl}_2\text{F}-\text{CClF}_2$  (CFC-113),  $\text{NO}_y$ ,  $\text{CO}_2$ ,  $\text{O}_3$ ,  $\text{CH}_4$ , and  $\text{H}_2\text{O}$  from the April-May 1993 deployment.  $\text{N}_2\text{O}$  was measured by tunable diode laser spectroscopy with the ATLAS instrument [Loewenstein *et al.*, 1990]; CFC-11, CFC-113, and  $\text{CH}_4$  by an airborne chromatograph for atmospheric trace species with the ACATS instrument [Woodbridge *et al.*, 1995],  $\text{NO}_y$  by a dual channel chemiluminescence detector [Fahey *et al.*, 1989];  $\text{CO}_2$  by an infrared analyzer [Boering *et al.*, 1994];  $\text{O}_3$  by a dual-beam UV absorption photometer [Proffitt *et al.*, 1989c]; and  $\text{H}_2\text{O}$  by a Lyman  $\alpha$  instrument [Kelly *et al.*, 1989]. Due to problems associated with temperature and pressure equilibration within the ATLAS instrument during SPADE, the first 45 min of  $\text{N}_2\text{O}$  data have been removed from the following analysis. These errors also resulted in a small positive bias for the remaining data relative to previous missions and to the ASHOE/MAESA campaign.

### 2.2. Tracer-Tracer Scatterplots

Plate 1 shows the scatterplots of CFC-11,  $\text{NO}_y$ ,  $\text{CO}_2$ ,  $\text{O}_3$ ,  $\text{CH}_4$ , and  $R_{\text{H}_2\text{O}} = \text{H}_2\text{O} - 2 \times (1.7 - \text{CH}_4)$  with  $\text{N}_2\text{O}$  for the April-May 1993 SPADE data; the different colors correspond to the different potential temperatures,  $\theta$ , of the measurements. Also shown, in some of the plots, are fits to data from other ER-2 campaigns (see caption for details). All scatterplots show linear relationships for  $\text{N}_2\text{O} < 240$  ppb, and, as will be argued below, are consistent with the sampled air being a mixture of polar and midlatitude air.

We first consider the CFC-11: $\text{N}_2\text{O}$  relationship, shown in Plate 1a. Also shown in Plate 1a is a fit to the data from AASE II; measurements from this campaign were made between October 1991 and March 1992, primarily in northern polar regions. (Data from whole air samples collected during AAOE, and AASE I and II, as well as results from two-dimensional chemical transport models, are similar to the AASE II curve [Kawa *et al.*, 1993; Woodbridge *et al.*, 1995].) A significant portion of the SPADE data (those with  $\text{N}_2\text{O} < 240$  ppb and CFC-11  $< 150$  ppt) deviates from the AASE II correlation curve. Note that reanalysis of the SPADE ATLAS  $\text{N}_2\text{O}$  data correcting for temperature and pressure differentials within the instrument should greatly reduce the difference between SPADE and AASE II data for  $\text{N}_2\text{O} > 240$  ppb. Also note that because the growth rates

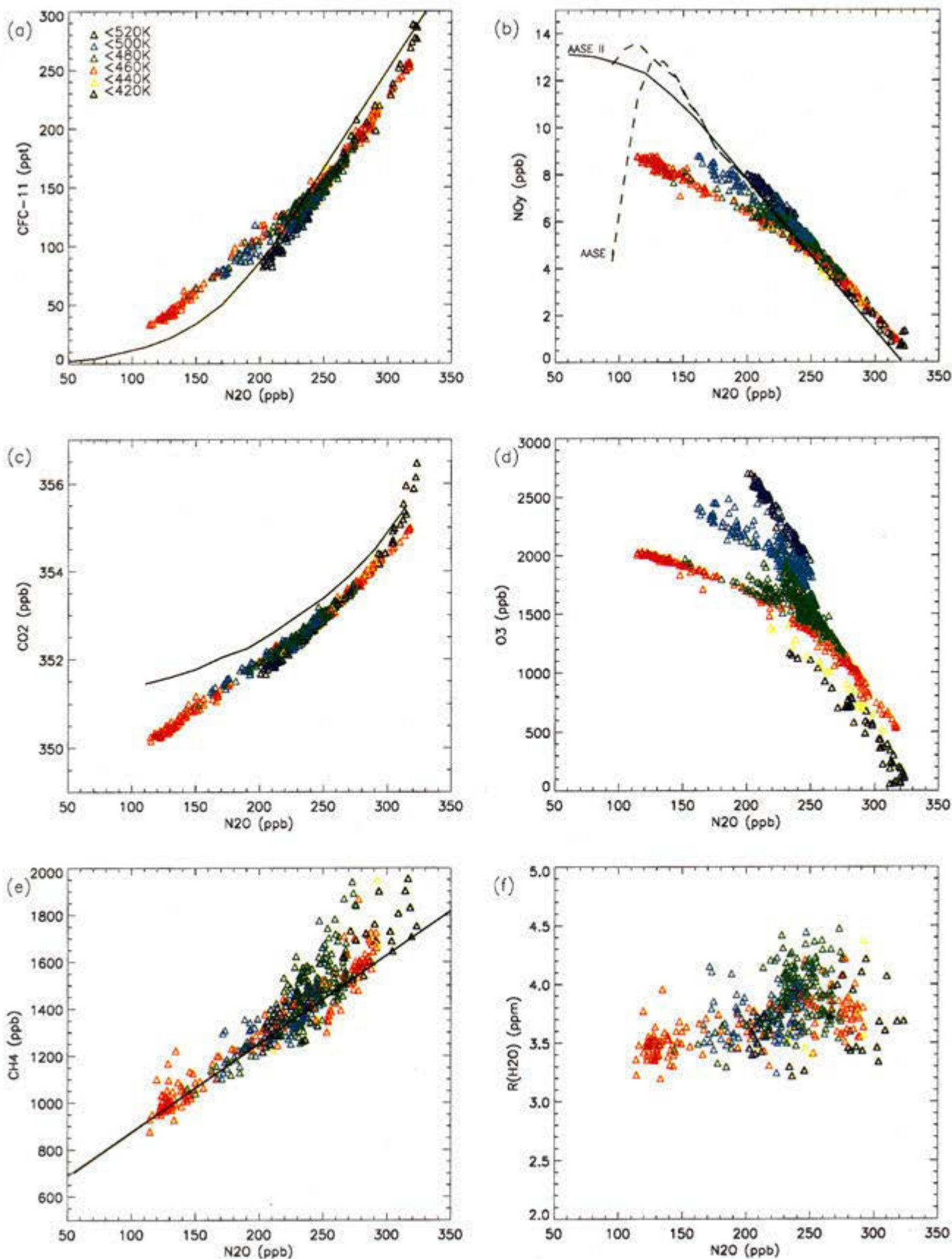


**Plate 1.** Scatterplot of (a) CFC-11, (b)  $NO_y$ , (c)  $CO_2$ , (d)  $O_3$ , (e)  $CH_4$ , and (f)  $R_{H_2O}$ , versus  $N_2O$  for data from the April-May 1993 flights of SPADE. The different colors correspond to the different  $\theta$  of the measurements (see legend in Plate 1a). The curves correspond to fits to the other ER-2 data: Plate 1a to AASE II, Plate 1b to AASE II (solid) and AASE I (dashed) curves: upper curve is for  $\theta = 470 \pm 10K$ , lower curve is for  $\theta = 450 \pm 10K$ , Plate 1c to the February 18, 1994 ASHOE/MAESA flight, and Plate 1e to AASE II data.

of the CFCs [Elkins *et al.*, 1993] have recently slowed down to near zero and the growth rate of  $N_2O$  is very small (0.2-0.3% per year [Elkins *et al.*, 1988]), there should be little change in the CFC-11: $N_2O$  correlation curve between the AASE II and SPADE campaigns. In the following, we refer to the correlation curves from AASE II (and earlier aircraft missions) as the "standard" correlation curve and to any data which do not fit on these curves as "anomalous" data. The anomalous CFC-11: $N_2O$  data from SPADE form a single straight line with no apparent  $\theta$  dependence.

Our hypothesis is that the anomalous SPADE data were the result of the mixing of two distinct airmasses, one airmass with low  $N_2O$  and CFC-11 (e.g., polar vortex air) and the other with high  $N_2O$  and CFC-11 (midlatitude air). The CFC-11: $N_2O$  ratio of the partially mixed air then lies on the straight line between the two original points on the scatterplot (see Figure 1). The SPADE data in Plate 1 lie along the line joining points on the standard correlation curve with  $N_2O \approx 80$  ppb and 240 ppb. (At the altitude of the measurements  $N_2O$  is  $\approx 160$  ppb at the vortex edge [Strahan and Mahlman, 1994].) Hence, if the anomalous data were caused by the above mixing scenario, these would be the values of  $N_2O$  of the unmixed polar and midlatitude air, respectively.

For low  $N_2O$ , the  $NO_y:N_2O$  scatterplot from SPADE also deviates from the correlation curves from previous aircraft campaigns, see Plate 1b (also shown is a fit to the AASE I data (dashed curves) and AASE II data (solid curve)). If the AASE II curve is considered as the standard curve, the SPADE  $NO_y:N_2O$  data appear to be inconsistent with the mixing of air with  $N_2O$  mixing ratios of 80 ppb and 240 ppb because the anomalous  $NO_y:N_2O$  data from SPADE are (1)  $\theta$  dependent, and (2) at  $\theta \approx 460$  K lie along the line joining  $N_2O = 240$  ppb and  $N_2O < 50$  ppb on the AASE II correlation curve (and not the line between  $N_2O = 240$  ppb and 80 ppb). However, these inconsistencies are removed if AASE I curves are considered the standard curves. The  $NO_y:N_2O$  correlation curves from AASE I are  $\theta$  dependent and show a dramatic decrease in  $NO_y$  for  $N_2O < 120$  ppb; thus, given the AASE I curves in Plate 1b, the  $\theta$  dependent mixing of air with  $N_2O$  mixing ratios of 80 ppb and 240 ppb could, in fact, account for the anomalous SPADE data observed in 1993.

The differences between the AASE I and AASE II  $NO_y$  data are believed to result from the sampling of denitrified air in February 1989 but not in February 1992 [Loewenstein *et al.*, 1993]. Therefore, if denitrification occurred during 1992/1993 (and was of a similar amount to that in 1988/1989), as suggested by other measurements (see below), then both the CFC-11: $N_2O$  and  $NO_y:N_2O$  data from SPADE suggest that the air sampled in spring 1993 was a mixture of two airmasses with distinct tracer values: one of polar origin ( $N_2O \approx 80$  ppb) and the other from middle latitudes ( $N_2O \approx 240$  ppb).

Measurements from earlier aircraft campaigns suggest that temperatures near the frost point are required for intense denitrification [Fahey *et al.*, 1990a]. Examination of analyzed temperatures shows that for short periods during the 1988/1989 and 1992/1993 winters the minimum temperature was around the frost point whereas the temperature everywhere remained above the frost point during the 1991/1992 winter (e.g., compare Figure 3b of Manney *et al.* [1994a] and Figure 4 of Fahey *et al.* [1990a]). Hence, the similarity between minimum temperatures in 1988/1989 and 1992/1993 then suggests that denitrification could also have occurred during 1992/1993. Furthermore, measurements of  $NO_y$  and  $N_2O$  by the atmospheric trace molecule spectroscopy (ATMOS) instrument during April 1993 indicate that denitrification had occurred in polar regions (H. Michelsen *et al.*, Evidence for aerosol-mediated repartitioning of halogen and nitrogen species in the lower stratosphere at northern midlatitudes, submitted to *Geophys. Res. Lett.*, 1996).

The  $CO_2:N_2O$  data, shown in Plate 1c, also support the mixing scenario outlined above. As in the case of CFC-11: $N_2O$ , the  $CO_2:N_2O$  scatterplot is bimodal for  $N_2O < 240$  ppb: data from air shown to be anomalous for CFC-11 and  $NO_y$  versus  $N_2O$  form a linear  $CO_2:N_2O$  correlation curve which deviate from the correlation curve for "non-anomalous" data. However, due to the dearth of nonanomalous data for  $N_2O < 240$  ppb and because an annual increase in tropospheric  $CO_2$  of 1-2 ppm/yr results in a yearly offset in  $CO_2:N_2O$  correlation plots [Boering *et al.*, 1994], it is difficult to predict what the "standard"  $CO_2:N_2O$  curve would have been during SPADE. Nevertheless, a fit to the ASHOE/MAESA test flight data from February 18, 1994 (solid curve, Plate 1c) is, in fact, nonlinear for  $N_2O < 240$  ppb, suggesting that the linear part of the  $CO_2:N_2O$  scatterplot is anomalous in the same sense as the linear portions of the CFC-11: $N_2O$  and  $NO_y:N_2O$  relationships are anomalous.

The  $O_3:N_2O$  scatterplot from SPADE has different anomalous straight lines for the different potential temperatures corresponding to the anomalous measurements (see Plate 1d). As in the case of  $NO_y:N_2O$ , the variation of  $O_3$  with  $\theta$  could be due to variations in the extent of chemical processing (and ozone loss) with altitude; therefore the  $O_3:N_2O$  data are also consistent with the mixing of vortex and midlatitude air. Assuming the linear correlation curves were produced by the mixing of air with  $N_2O = 80$  and 240 ppb (as implied by the CFC-11: $N_2O$  data) we have, from Plate 1d, that the  $O_3$  mixing ratio of the unmixed air with  $N_2O = 80$  ppb, at  $\theta = 460$  K, was around 2200 ppb. This is significantly less  $O_3$  than measured in 1992 for the same  $N_2O$  and  $\theta$  during AASE II (see Figure 2 of Proffitt *et al.* [1993]), and is consistent with the analysis of Manney *et al.* [1994a] which showed greater Arctic ozone loss in 1993 than in 1992. Thus the SPADE  $O_3:N_2O$  data suggest that there has been ozone destruction and that this ozone-

depleted air is mixed into middle latitudes during the break-up of the vortex. However, the quantification of this effect through the tracer-tracer correlations is likely complicated by the timescales for  $O_3$  chemistry relative to transport [Plumb and Ko, 1992; Hall and Prather, 1995].

The  $CH_4:N_2O$  scatterplot from SPADE (Plate 1e) forms a linear correlation curve, but the data are not anomalous compared to previous campaigns (the solid curve is a fit to AASE II [Kawa et al., 1993]). This is because the standard  $CH_4:N_2O$  correlation curve is linear for  $N_2O > 80$  ppb, and therefore the mixing of polar air ( $N_2O \approx 80$  ppb) with middle latitude air does not alter this correlation (see Figure 1).

Residual water  $R_{H_2O}$  is approximately conserved in the stratosphere except when dehydration occurs [Kelly et al., 1989; Fahey et al., 1990a; Tuck et al., 1994]. Plate 1f shows the scatterplot of  $R_{H_2O}$  against  $N_2O$ . The measured  $R_{H_2O}$  during SPADE is relatively constant (3.3–3.9 ppm) for  $N_2O < 240$  ppb, with only a slight variation with  $N_2O$ . This lack of variation indicates that there had been very little (if any) dehydration of the sampled air. As noted above, the  $NO_y:N_2O$  scatterplot suggests that this air had been denitrified. Hence the scatterplots suggest that in the “anomalous” air there was denitrification without dehydration; this is consistent with the air sampled during AASE I [Fahey et al., 1990a].

### 2.3. Spatial Distribution

The anomalous correlation curves discussed above occur for low values of  $N_2O$  ( $< 240$  ppb) measured from several SPADE flights. The majority are from the flight of May 7, with the remainder from the flights of April 30, May 1, and May 6. The spatial distribution of the measurements of low  $N_2O$  on these flights is now discussed. Note that on the flights of April 23 and 26 low  $N_2O$  and  $CO_2$  were also measured [Newman et al., 1996] but there were no corresponding measurements of CFC-11 or  $NO_y$ .

The May 7 flight was a “racetrack” pattern consisting of seven near-isentropic legs between ( $36.5^\circ N, 125.5^\circ W$ ) and ( $37.5^\circ N, 122^\circ W$ ). The first five legs were at  $\theta \approx 460$  K, and the last two at  $\theta \approx 490$  K. Low values of tropospheric source gases (e.g.,  $N_2O < 180$  ppb) were measured on all legs. The location of the low- $N_2O$  air differed between legs but was generally at the most southern point of each leg, and the aircraft turned around in this low- $N_2O$  air. On the final two legs low  $N_2O$  was measured, in regions approximately 100 km wide, in the middle of the legs, and the aircraft passed completely through the low- $N_2O$  air. A region of low  $N_2O$  was also sampled at  $\theta \approx 450$  K during the final descent. The structure of the transition from low to high  $N_2O$  varied among encounters with all showing fine-scale features.

On both the April 30 and May 1 flights, low values of  $N_2O$  were measured in a narrow altitude range ( $\Delta\theta \approx$

10K) while the ER-2 was ascending and descending:  $\theta \approx 450$  K above Ames ( $37.5^\circ N, 122^\circ W$ ) on April 30 (see Figure 2 of Newman et al. [1996]), and  $\theta \approx 465$  K at  $60^\circ N, 125^\circ W$  on May 1. On the flight of May 6 a narrow region (with horizontal extent around 300 km) of low  $N_2O$  was measured as the ER-2 climbed from  $\theta = 455$  K to  $\theta = 500$  K. On the remainder of all three flights the measured  $N_2O$  was greater than 240 ppb.

The above measurements of low  $N_2O$  suggest that during SPADE the ER-2 passed through several localized regions of exvortex air. During the earlier flights of April 30 and May 1 narrow regions of exvortex air were sampled only when the aircraft ascended or descended through altitudes corresponding to  $\theta \approx 460$  K and not at higher or lower altitudes. In contrast, on the flights of May 6 and 7 the ER-2 flew “horizontally” into the exvortex air over a range of altitudes ( $450 \text{ K} < \theta < 500 \text{ K}$ ).

### 3. Evolution of the Polar Vortex During 1992/1993

In the previous section, we suggested that the anomalous air sampled during SPADE comprised a mixture of exvortex and midlatitude air. We now examine the evolution of the polar vortex in the lower stratosphere during the 1992/1993 winter and investigate when the mixing of polar vortex and midlatitude air occurred.

In early 1993 the Arctic polar vortex remained a single entity in the lower stratosphere until mid-April. Maps of Ertel’s potential vorticity (PV) on isentropic surfaces show a strong coherent vortex throughout this period with no sign of any large-scale mixing events inside the vortex. Figure 2 shows the temporal evolution of the area enclosed by PV contours, derived from National Meteorological Center (NMC) analyses, on the 460 K isentropic surface for the first five months of 1993.

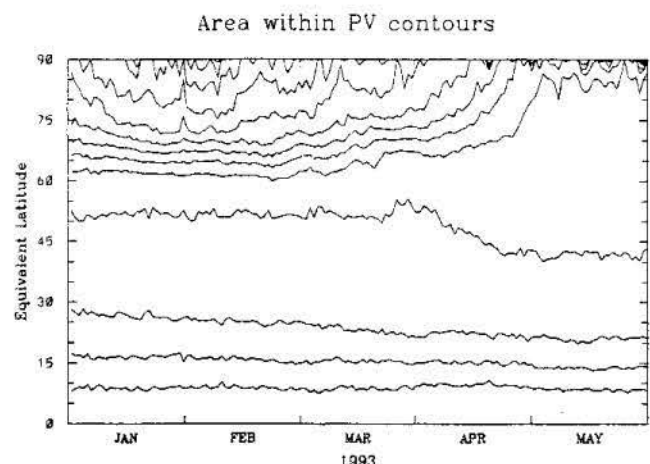


**Figure 2.** Temporal evolution of the equivalent latitude of PV contours on the 460 K isentropic surface, from NMC analyses, for January to May 1993. Lower contour is  $0.5 \times 10^{-5} \text{ Km}^2 \text{ s}^{-1} \text{ kg}^{-1}$ ; interval is  $0.5 \times 10^{-5} \text{ Km}^2 \text{ s}^{-1} \text{ kg}^{-1}$ .

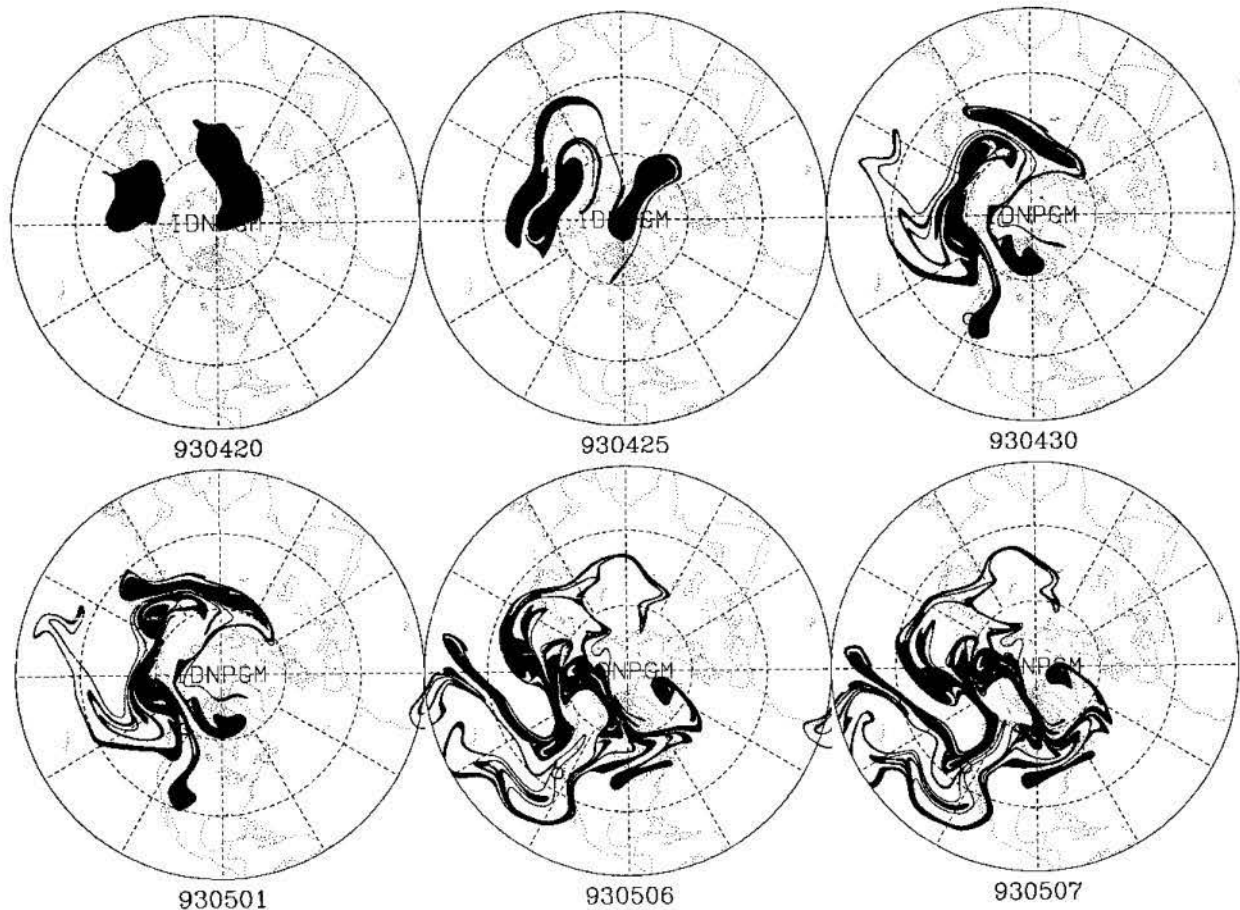


**Figure 3.** Contour advection calculation on the 460 K surface using NMC winds for April 20 to May 7, 1993. Contour was initialised as  $PV=2.4 \times 10^{-5} \text{K m}^2 \text{s}^{-1} \text{kg}^{-1}$  contour on April 20. Circles mark locations where low  $\text{N}_2\text{O}$  was measured. Outer edge of map is  $10^\circ\text{N}$ .

The closeness of the contours in Figure 2 is an indicator of the steepness of PV gradients (and the edge of the vortex). The size of the vortex remained approximately constant from January until the end of March and then decreased during the breakup of the vortex (note that the temperatures inside the vortex were rapidly increasing during the above period). Contour advection (CA) calculations [Waugh and Plumb, 1994; Norton, 1994] using NMC analyses confirm that that air was not transported out of or into the vortex during the January to mid-April period (although air was peeled from the outer edges of the vortex in Rossby wave breaking events). Manney *et al.* [1994b] have also shown, using PV analyses together with three-dimensional trajectory calculations, that the polar vortex was isolated at 465 K during the 1992/1993 winter.

After the breakup of the polar vortex there was vigorous mixing of vortex and midlatitude air. In the lower stratosphere, the polar vortex broke up into several fragments around April 18, and these fragments dissipated during the last 2 weeks of April [e.g., Nash *et al.*, 1996; Newman *et al.*, 1996]. Figure 3 shows a CA calculation on the 460 K surface (which was initialized with the two largest fragments of the polar vortex on April

20) showing the fine-scale transport during this period. This calculation indicates that after the break-up there was strong stirring (mixing), and the fragments of the vortex were stretched into long thin filaments which became very convoluted. These filaments of exvortex air were advected over the North Pacific and western United States during the April/May SPADE campaign period but not over Europe.

The evolution on other surfaces between 440 K and 500 K is qualitatively the same as at 460 K, with the exvortex air stretched into long, convoluted, filamentary structures. There are, however, some important differences. In particular, the filaments on different isentropic surfaces are generally not vertically aligned; e.g., compare Figure 4, which shows the evolution on the 490 K surface, with Figure 3. In other words, the filaments on isentropic surfaces are in fact sloping sheets. During the period shown in Figures 3 and 4 the sheets of exvortex air slope westward with increasing height (see also Plate 5 of Newman *et al.* [1996]), and the exvortex air arrives over the SPADE measurement sites earlier at the lower altitude, e.g., April 30 at 460 K compared with May 6 at 490 K (see Figures 3 and 4).

The evolution of the exvortex air in the CA calcu-

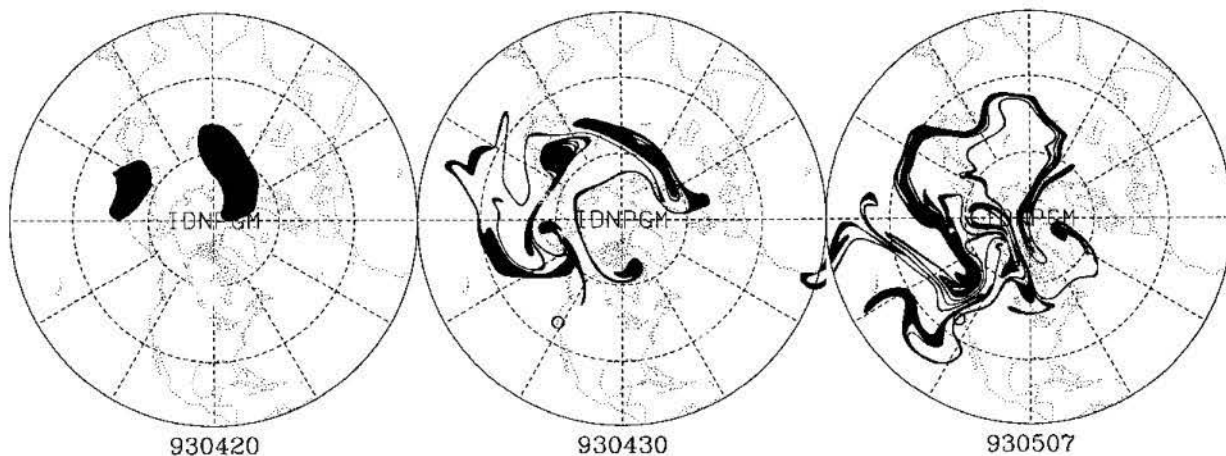


Figure 4. As in Figure 3 except on the 490 K surface; initial contour is  $PV=3.5 \times 10^{-5} \text{Km}^2 \text{s}^{-1} \text{kg}^{-1}$  contour.

lations is consistent with the SPADE measurements of low  $\text{N}_2\text{O}$ . As discussed in section 2.3, during early ER-2 flights (April 30 and May 1) low  $\text{N}_2\text{O}$  was observed only when the aircraft was at  $\theta \approx 460 \text{ K}$ , while on later flights (May 6 and 7) low  $\text{N}_2\text{O}$  was measured at all altitudes between 440 K and 500 K. There is good qualitative agreement between the location of the filaments (sheets) of exvortex air in the CA calculations and the location of the measurements of low  $\text{N}_2\text{O}$  (see the circles in Figures 3 and 4). However, there is not exact agreement. The differences are probably due to inaccuracies in the winds. CA calculations have also been performed with winds from the NASA Goddard Space Flight Center (GSFC) GEOS 1 assimilation [Schubert *et al.*, 1993] and the United Kingdom Meteorological Office (UKMO) UARS stratospheric assimilation [Swinbank and O'Neill, 1994]. These calculations produce similar filamentary structures to those described above, but there are differences in the exact structure and location of the filaments of exvortex air (see also Newman *et al.* [1996]). However the different CA calculations all suggest that the low- $\text{N}_2\text{O}$  air sampled on the May 6 and 7 flights was part of a sheet of air produced during the "shearing out" of the vortex fragment over China that occurred around April 25 (see Figure 3). This implies that around 12 days had lapsed since the sheet was created.

#### 4. Mixing in a Strain-Diffusion Model

We have argued above that the linear correlation curves for long-lived tracers measured during SPADE are the result of the mixing of two air masses with distinct tracer values, namely, the mixing of a filament of vortex air into middle latitudes. However, it is possible that the data are the result of mixing of air with a broad range of tracer values. To examine the effect of the initial distribution of the tracers on the tracer-tracer scatterplots of the resultant "mixed" distribution, we ex-

amine the mixing of tracers in a one-dimensional strain-diffusion model.

This strain-diffusion model is that used by Prather and Jaffe [1990]. In this model the temporal evolution of the tracer concentration  $\sigma(\mathbf{x}, t)$  is governed by the equations

$$\frac{\partial \sigma}{\partial t} = D \frac{\partial^2 \sigma}{\partial x^2}, \quad (1)$$

$$\Delta \mathbf{x}(t) = \Delta \mathbf{x}(0) \exp(-St), \quad (2)$$

where  $\Delta \mathbf{x}$  is the spacing of the uniform grid used in the  $\mathbf{x}$  dimension. Equation (1) models the effect of diffusion across the air mass ( $D$  is the diffusion coefficient), while equation (2) models the effect of random strain ( $S$  is the rate of strain), see Prather and Jaffe [1990] for further

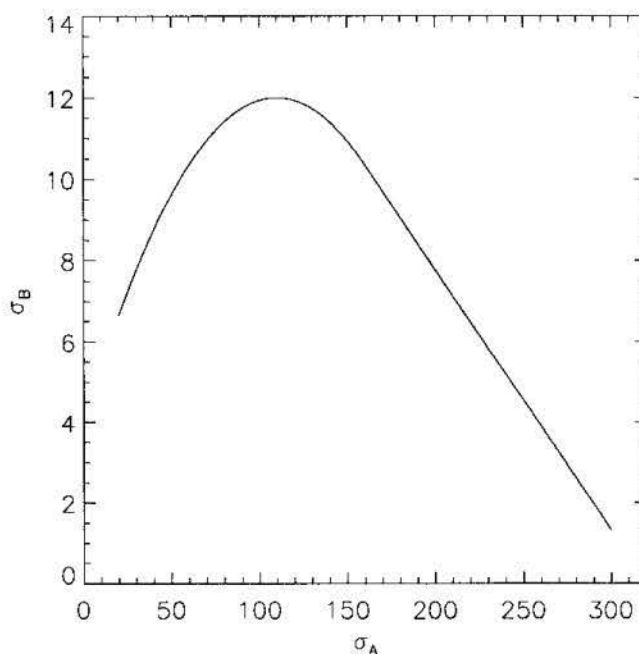
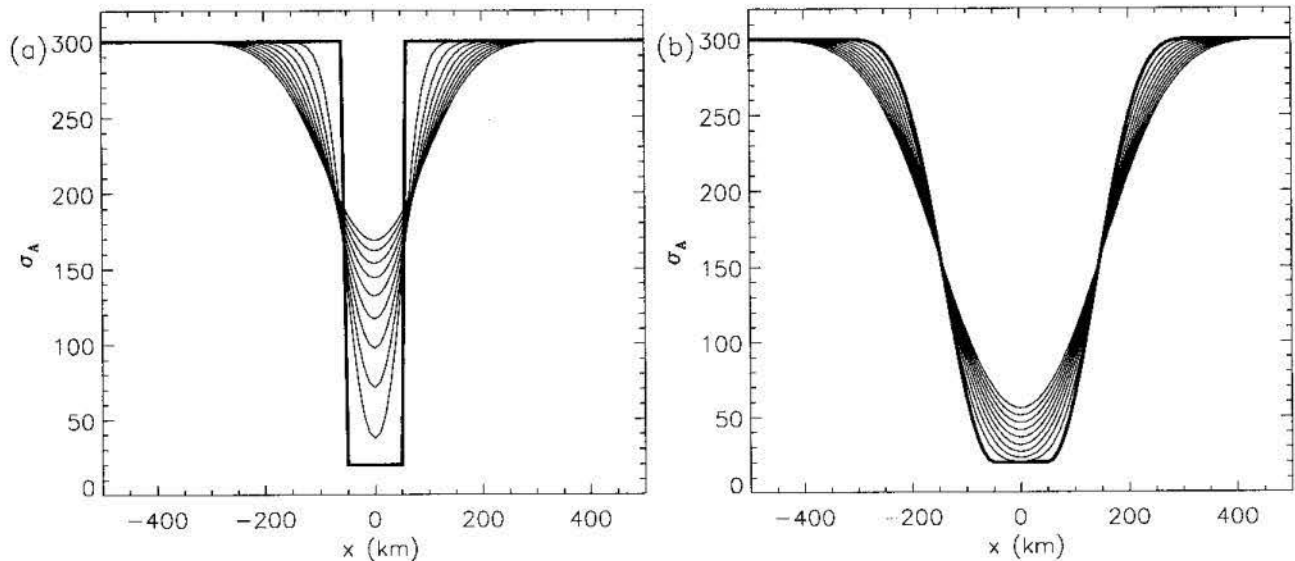


Figure 5. A:B correlation curve for initial profiles in the strain-diffusion model.



**Figure 6.** The temporal evolution of tracer concentration  $\sigma_A$  in the strain-diffusion model for (a) the top hat distribution and (b) the broad distribution. In these calculations there is no strain ( $S=0$ ) and  $D = 5 \times 10^3 \text{m}^2/\text{s}$ . Bold curve is initial profile, and profiles are shown at daily intervals.

details. Prather and Jaffe considered strain and diffusion in the vertical, and used values of  $D$  representative of molecular diffusion. Here we consider strain-diffusion in the horizontal, and  $D$  corresponds to the effective horizontal diffusion produced by three-dimensional mixing processes, rather than the coefficient of molecular diffusion. In other words, we are assuming (for simplicity) that the three-dimensional mixing can be modeled using simple diffusion in the horizontal.

We consider the evolution of two tracers A and B, with concentrations  $\sigma_A$  and  $\sigma_B$ . The initial profiles of these tracers are chosen so that the  $\sigma_A:\sigma_B$  ratio lies on the curve shown in Figure 5. (Here we are considering A as a  $\text{N}_2\text{O}$ -like tracer and B as a  $\text{NO}_y$ -like tracer.) Initially the minimum value of  $\sigma_A$  (which, for a  $\text{N}_2\text{O}$ -like tracer, corresponds to the most poleward air) is at  $x = 0$ , and the profile is symmetric about  $x = 0$ . We consider a range of initial  $\sigma_A$  profiles ranging from a “top hat” profile (corresponding to a filament of constant concentration in a constant background) to a “broad” (Gaussian-like) profile (see Figure 6, bold curves). Given initial  $\sigma_A$ , the initial profile of  $\sigma_B$  is then determined from the correlation curve shown in Figure 5. The temporal evolution of  $\sigma_A$  and  $\sigma_B$  (and hence the A:B scatter plot) is then determined by solving equations (1) and (2) numerically.

Figure 6 shows the evolution of the profile of  $\sigma_A$ , in the case of no strain (i.e.  $S = 0$ ), for the initial top hat profile and broad profile. The corresponding evolution of A:B scatterplots are shown in Figure 7a (top hat) and 7b (broad). These plots show clearly that the tracer-tracer scatterplots formed from the (diffusive) mixing of two distinct airmasses are very different from those formed by mixing an initially broad distribution of tracer values. Mixing two distinct airmasses

produces a linear correlation curve along the line joining the two original points on the scatter plot, whereas mixing a broad distribution “flattens out” the nonlinear correlation curve as the mixing proceeds. Note that as the mixing proceeds the tracer values move from the interior air values (low  $\sigma_A$ ) toward the exterior values (high  $\sigma_A$ ). The rate of movement of this end value depends on  $D$  (i.e., for larger  $D$  the minimum value increases more rapidly). Similar calculations have been performed with nonzero strain. The evolution of the tracer-tracer relationship for the different profiles is similar (with the rate of change of the correlation curves now depending on both  $D$  and  $S$ ). Comparing the results of the strain-diffusion model (Figure 7) with the tracer-tracer scatterplots from SPADE (Plate 1) provides further support for the hypothesis that the air sampled during SPADE was the result of mixing a filament of polar air into a middle latitude airmass, rather than mixing air with a broad range of tracer values.

We now consider in more detail the mixing of a filament into a uniform background in the strain-diffusion model. Prather and Jaffe [1990] showed that the results from this model are sensitive to the values of  $S$  and  $D$ . Here we use the tracer observations from SPADE together with CA calculations to infer appropriate values of  $S$  and  $D$  for the transport/mixing during SPADE.

The appropriate value of  $S$  for the SPADE time period can be estimated from the rate of growth of the contour length in the CA calculations [e.g., Pierce and Fairlie, 1993]. Equation (2) models the exponential reduction in the minimum dimension of air parcels due to random straining. Assuming conservation of area (which is true for incompressible, nondivergent flow, and is a reasonable assumption for flow in the lower stratosphere), this then corresponds to exponential increase, with the

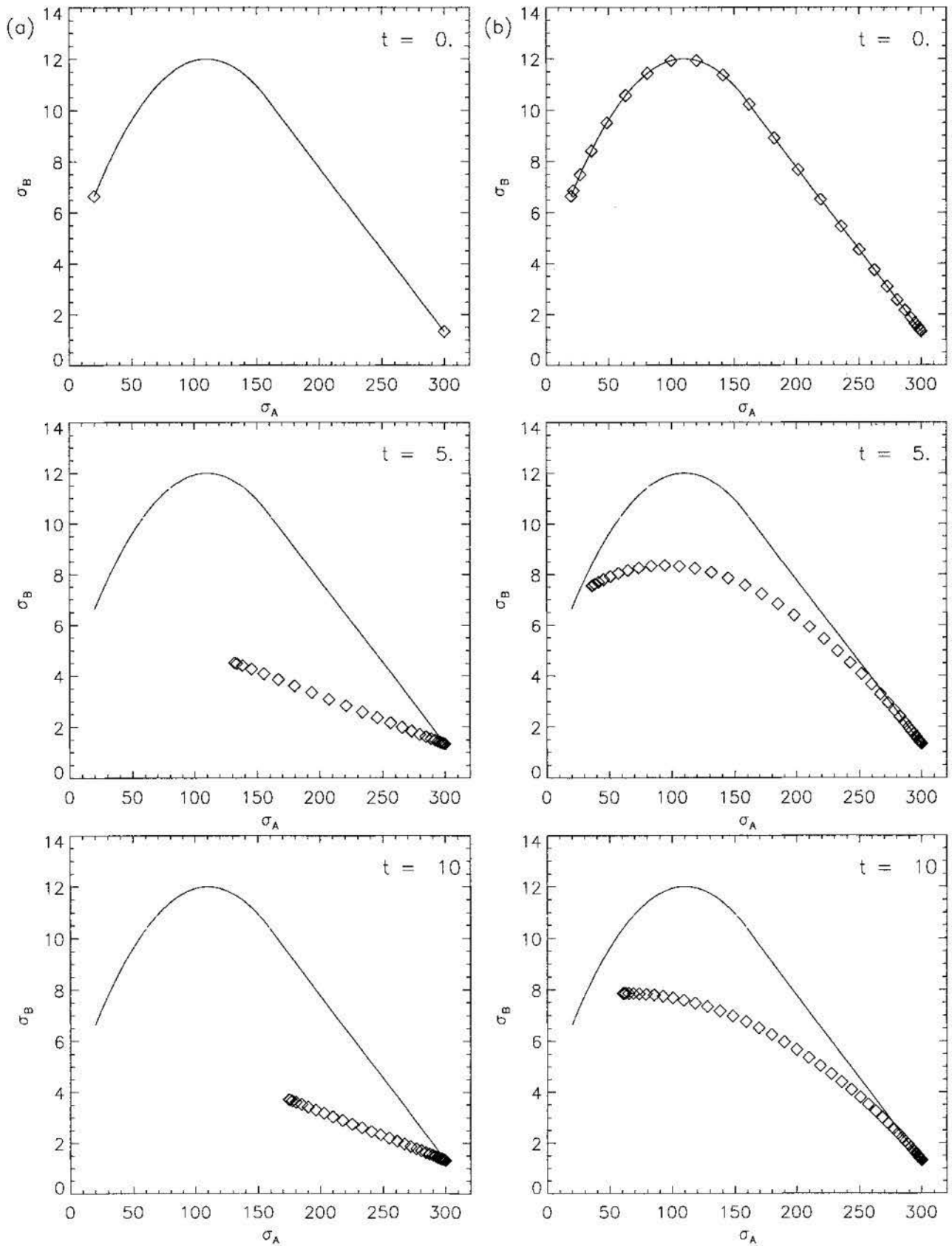
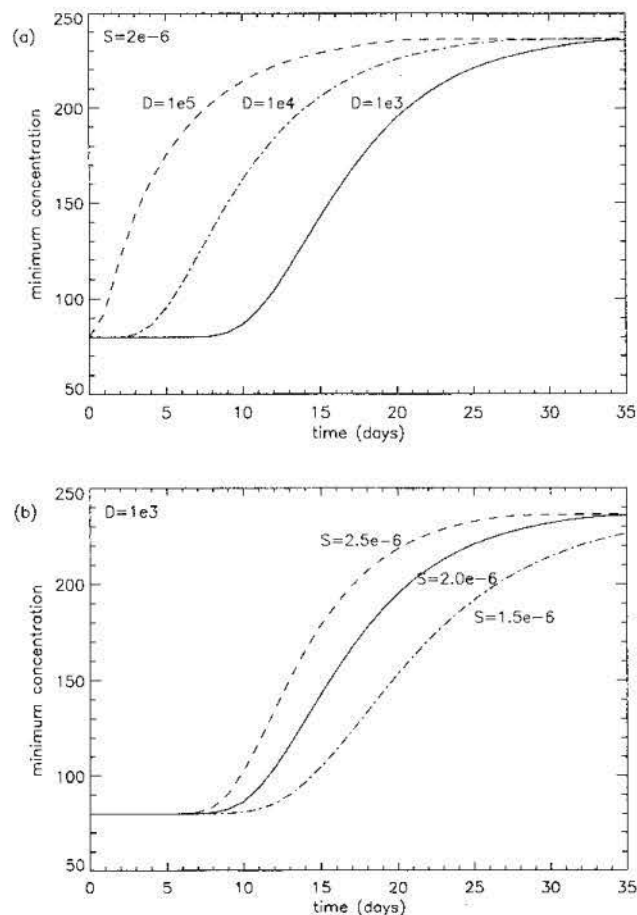


Figure 7. A:B scatterplots for the tracer profiles shown in figure 6, at 5 day intervals.

same exponent  $S$ , of the length of contours in CA calculations. The length of contours in the CA calculations described in section 3 does increase approximately exponentially, and so this supports the use of the above strain model. The value of  $S$  determined from the calculations with NMC winds varies only slightly with initial PV contour and isentropic surface (for  $450\text{ K} < \theta < 500\text{ K}$ ), with  $S$  between  $2.0 \times 10^{-6}\text{ s}^{-1}$  and  $2.5 \times 10^{-6}\text{ s}^{-1}$ . The insensitivity of the stretching rate to the latitude of the initial contour implies approximately constant stirring throughout middle and high latitudes, and is in contrast to midwinter calculations in which there is a minimum in the stretching rate near the vortex edge [e.g., Pierce and Fairlie, 1993; Chen, 1994]. Calculations using UKMO winds yield similar stretching rates to those using NMC winds, but calculations with GSFC winds produce greater stirring (with  $S \approx 3 \times 10^{-6}\text{ s}^{-1}$ ).

The minimum  $\text{N}_2\text{O}$  measured on the May 7 flight was approximately 115 ppb; the fact that the CFC-11: $\text{N}_2\text{O}$  data lie on a line joining the standard curve at 80 ppb indicates that the  $\text{N}_2\text{O}$  value at the interior of the filament has changed from 80 ppb to 115 ppb. Furthermore, CA calculations (see section 3) indicate that the filament formed around 12 days earlier and therefore



**Figure 8.** Temporal evolution of minimum  $\sigma_A$  for (a)  $S = 2 \times 10^{-6}\text{ s}^{-1}$ ,  $D = \{10^3, 10^4, 10^5\}\text{ m}^2/\text{s}$  and (b)  $S = \{1.5, 2.0, 2.5\} \times 10^{-6}\text{ s}^{-1}$ ,  $D = 10^3\text{ m}^2/\text{s}$

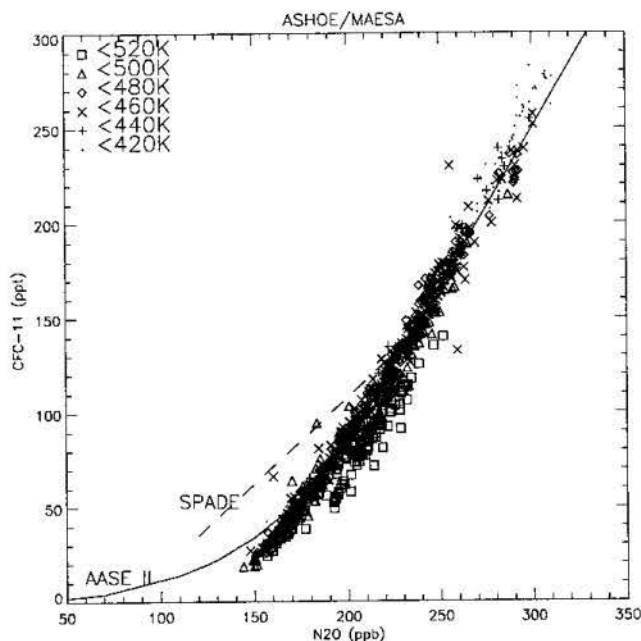


**Figure 9.** Scatterplot of CFC-11 versus  $\text{N}_2\text{O}$  for southern hemisphere data from all four deployments of ASHOE/MAESA. The solid curve is a fit to the AASE II data; dashed curve is a fit to the anomalous data from SPADE (see Plate 1).

suggest that the above mixing occurred in around 12 days. As noted above, in the strain-diffusion model the rate of change of the minimum value depends on  $S$  and  $D$ . Using the above estimate of  $S$ , together with the observation that the interior value mixed upward from 80 ppb to 115 ppb in around 12 days, we can estimate the appropriate value of  $D$  in the strain-diffusion model.

Figure 8 shows the temporal evolution of the minimum  $\sigma_A$  for calculations with several values of  $S$  and  $D$ , for an initial filament of width  $\delta_0 = 500\text{ km}$  (the approximate width of the filament on April 25) with  $\sigma_A = 80\text{ ppb}$  inside and  $\sigma_A = 240\text{ ppb}$  outside. For  $S$  between  $2.0 \times 10^{-6}\text{ s}^{-1}$  and  $2.5 \times 10^{-6}\text{ s}^{-1}$ , the minimum value increases from 80 to 115 in around 12 days if  $D \approx 10^3\text{ m}^2/\text{s}$ . With this value of  $D$ , the extreme value inside the filament does not change for the first 7-8 days, then changes rapidly in the next 15 days as the filament is stretched out and mixes with the background air; in approximately 30 days, the filament is completely mixed with the background air. Thus these calculations suggest that after the break up of the Arctic vortex the air from inside the vortex is completely mixed into the middle latitude within a month.

There are, of course, large uncertainties in the values of each of the parameters used in the above calculations, and the mixing rate is sensitive to these parameters, as shown in Figure 9 (see also Prather and Jaffe [1990]). Note, however, M. G. Balluch and P. H. Haynes (Quantification of lower stratospheric mixing processes using aircraft data, submitted to *Journal of Geophysical Research*, 1996) recently examined the SPADE data using

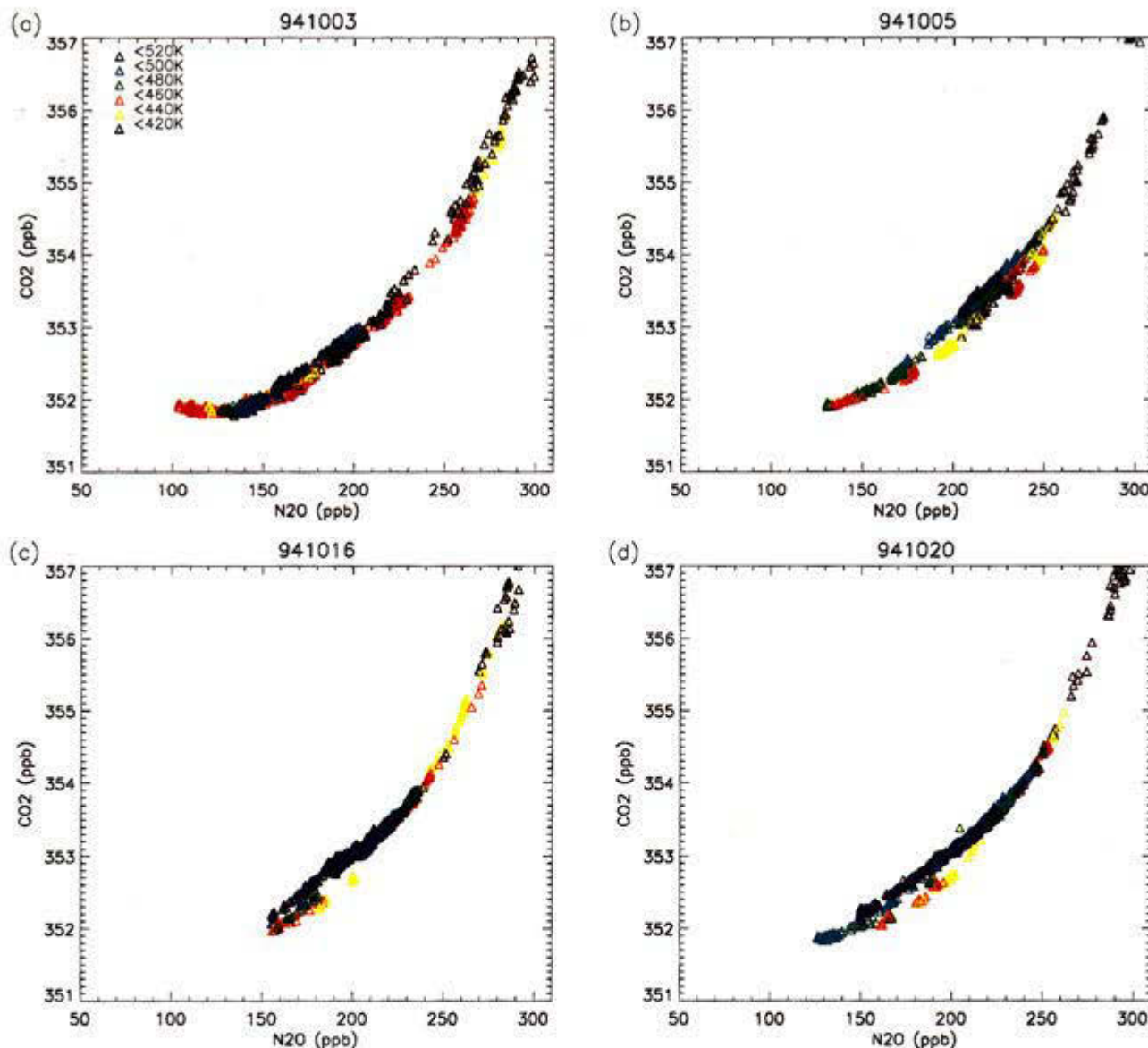


**Plate 2.** Scatterplot of  $\text{CO}_2$  versus  $\text{N}_2\text{O}$  for data from ASHOE/MAESA flights on (a) October 3, (b) October 5, (c) October 16, and (d) October 20, 1994. The different colors correspond to different  $\theta$  bins.

a different technique, and their estimate of the diffusivity is consistent with the above value.

## 5. ASHOE/MAESA Measurements

We now examine the tracer-tracer interrelationships observed during the ASHOE/MAESA campaign, and compare these with the relationships from SPADE and earlier campaigns. ASHOE/MAESA comprised four deployments based in Christchurch, New Zealand ( $43^\circ\text{S}$ ,  $172^\circ\text{E}$ ) and spanned a 9 month period from February to November 1994. The measurements were obtained with the same instruments as the SPADE data (see section 2.1), except CFC-11 which was measured by the ACATS IV instrument [Elkins *et al.*, 1996].

Throughout the four deployments, the scatterplots of CFC-11: $\text{N}_2\text{O}$  (Figure 9) and  $\text{NO}_y$ : $\text{N}_2\text{O}$  [see Keim *et*

*al.*, this issue] show no evidence for the anomalous mixing of low- $\text{N}_2\text{O}$  air with midlatitude air observed during SPADE. (Note that there is a systematic shift in the  $\text{NO}_y$ : $\text{N}_2\text{O}$  correlation curves between the different deployments [Keim *et al.*, this issue], but this variation is much smaller than that produced by recent mixing of vortex and midlatitude air.) However, multiple,  $\theta$ -dependent, mixing lines do appear in the  $\text{CO}_2$ : $\text{N}_2\text{O}$  scatterplots from the October deployment for  $\text{N}_2\text{O} < 240$  ppb (see Plate 2). These mixing lines are not apparent in the  $\text{CO}_2$ : $\text{N}_2\text{O}$  scatterplots from the three other deployments (not shown), although their existence cannot be completely ruled out for the third deployment in July/August 1994 since there is a slightly different correlation for data with  $\theta < 420$  K than for  $\theta > 420$  K, and undersampling (both spatially and in  $\text{N}_2\text{O}$  space) may be of concern. Also, data from the March-April

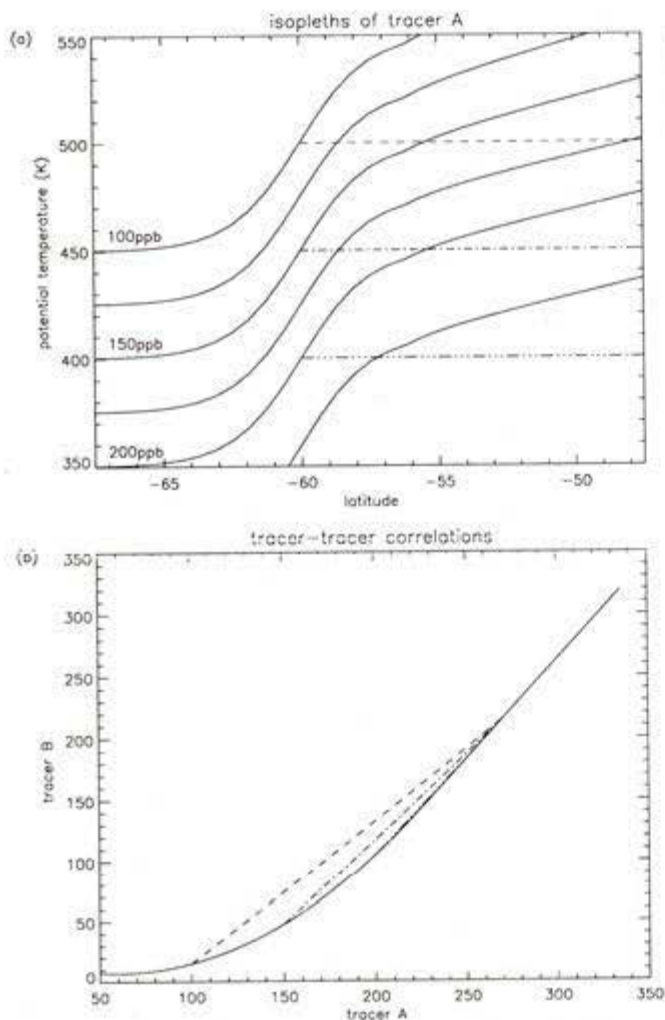


**Figure 10.** (a) Potential temperature - latitude cross-section of a  $N_2O$ -like tracer A. The dashed horizontal lines represent the range of isentropic mixing. (b) Tracer-tracer scatterplots of tracer A and tracer B (a  $CO_2$ -like tracer). The solid curve represents the standard correlation curve, whereas the dashed curves represent the “mixing lines” produced by isentropic mixing at 500 K, 450 K, and 400 K (see dashed lines in Figure 10a).

flights out of Christchurch before the spin-up of the vortex show a bimodal distribution; this distribution is not indicative of the mixing processes discussed in this paper but, rather, appear to be similar to the “pressure bands” in the three-dimensional modeling study of *Hall and Prather* [1995].

The tracer-tracer scatterplots from the fourth deployment raise two interesting questions. First, why are there mixing lines in the  $CO_2:N_2O$  scatterplot but not in the scatterplots of other long-lived tracers (such as  $NO_y:N_2O$  and  $CFC-11:N_2O$ )? Second, why are the mixing lines  $\theta$  dependent?

The absence of mixing lines in other long-lived tracers is due to their standard correlation curves (with  $N_2O$ ) being approximately linear for the range of  $N_2O$  affected by the mixing ( $N_2O > \approx 120$  ppb), whereas the stan-

dard  $CO_2:N_2O$  correlation curve is nonlinear within this range. Hence the mixing of vortex edge air ( $N_2O \approx 120$  ppb) with midlatitude air does not alter the  $NO_y:N_2O$  and  $CFC-11:N_2O$  correlation curves but it does change the  $CO_2:N_2O$  correlation curve. This is the same reason why mixing lines are detected in the  $NO_y:N_2O$  and  $CFC-11:N_2O$  scatterplots from SPADE, but not in the corresponding  $CH_4:N_2O$  scatterplot (see Plate 1).

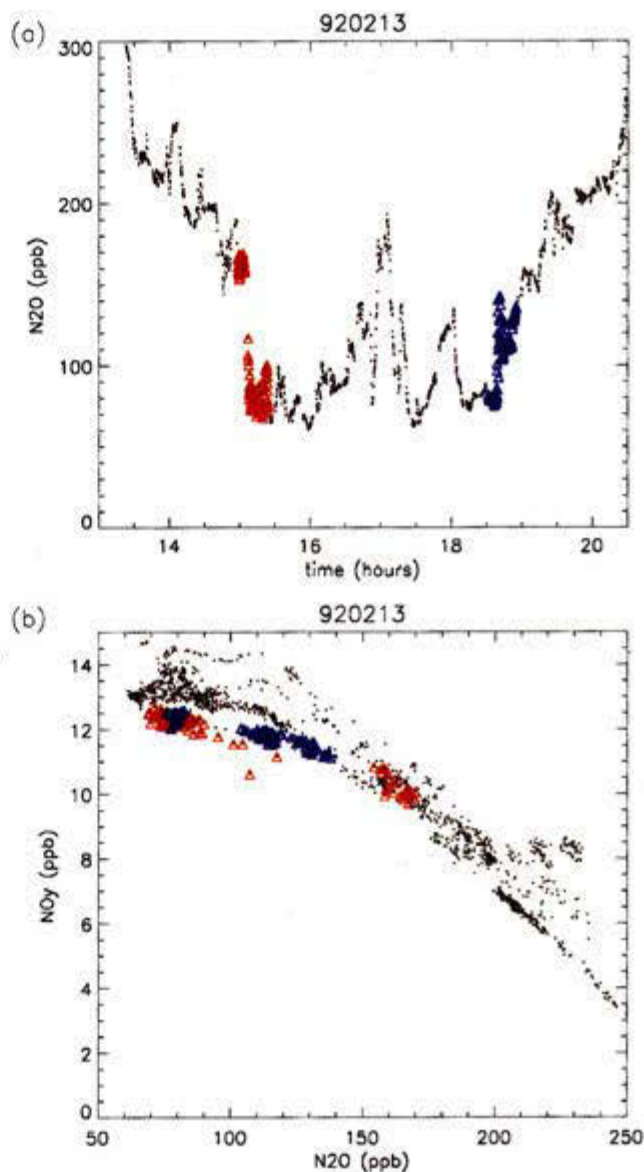


**Plate 3.** Data from AASE II flight on February 13, 1992: (top) time series of  $N_2O$ ; (bottom) scatterplot of  $NO_y:N_2O$ . The colored symbols are the data that form the mixing lines: the blue symbols correspond to data measured within the vortex edge region during the poleward leg into the vortex, while the orange symbols correspond to data measured within the vortex edge region during the return leg out of the vortex. Note that some of the scatter in the  $NO_y:N_2O$  could be attributable to the temperature/pressure dependence of the ATLAS instrument during AASE II.

The  $\theta$  dependence of the  $\text{CO}_2\text{:N}_2\text{O}$  mixing lines is probably related to the strong  $\theta$  dependence of the tracer concentrations. The values of tropospheric source gases, such as  $\text{N}_2\text{O}$  and  $\text{CO}_2$ , decrease with increasing altitude at the vortex edge (e.g., in September 1987 (AAOE)  $\partial\text{N}_2\text{O}/\partial\theta \approx -0.8$  ppb/K [Strahan and Mahlman, 1994]). Isentropic transport/mixing, which is generally confined to the region between the steep gradients at the vortex edge and the steep subtropical gradients (the so-called surf zone), therefore mixes lower values of  $\text{N}_2\text{O}$  into middle latitudes, and reaches further into the nonlinear section of the correlation curve, at higher potential temperatures, as shown schematically in Figure 10. In other words, transport/mixing along the 500 K surface, for example, may mix air masses from the nonlinear section of the  $\text{CO}_2\text{:N}_2\text{O}$  correlation curve, whereas transport/mixing along the 450 K surface may only mix air masses within the linear region (e.g., compare Figures 10a and 10b). The observed variation of the intersection of the mixing lines with the "standard" (nonlinear)  $\text{CO}_2\text{:N}_2\text{O}$  correlation as a function of potential temperature in Plate 2 is consistent with the schematic in Figure 10; at 500 K the mixing lines intercept the nonlinear portion of the  $\text{CO}_2\text{:N}_2\text{O}$  correlation curve at  $\text{N}_2\text{O} \approx 140$  ppb, whereas at 460 K the intercept is at  $\text{N}_2\text{O} \approx 170$  ppb.

Thus, the October scatterplots show that the mixing of vortex "edge" air into midlatitudes has occurred (from  $\text{CO}_2\text{:N}_2\text{O}$ ) but that mixing of inner vortex air into midlatitudes has not occurred (from  $\text{CFC-11:N}_2\text{O}$  and  $\text{NO}_y\text{:N}_2\text{O}$ ).

## 6. Discussion and Conclusions

The presence of anomalous lines in scatterplots of tracers without significant local chemical losses proves to be a direct indicator of anomalous mixing processes. Different tracer pairs exhibit curvature in different locations in physical space and allow us to diagnose mixing at different locations and times. The power of this approach is that interpretation is relatively unambiguous. In the tracers shown, except  $\text{O}_3$  (and  $\text{NO}_y$  when denitrification has occurred), chemical causes can be ruled out because of the rapidity of the changes. More importantly, the approach is insensitive to how the mixing takes place: issues such as the competition between diabatic advection and isentropic mixing, which can cloud interpretation, do not arise here; all that matters is the mixing ratios (or range of mixing ratios) in the air masses being mixed.

As mentioned in the introduction, the scatterplots of  $\text{NO}_y\text{:N}_2\text{O}$  and  $\text{CFC-11:N}_2\text{O}$  from the winter flights from AAOE, AASE I, and AASE II form compact correlations (except for  $\text{NO}_y\text{:N}_2\text{O}$  inside the vortex when denitrification has occurred). Further examination of these data show anomalous mixing lines on one flight: there are mixing lines in the  $\text{NO}_y\text{:N}_2\text{O}$  scatterplot for data measured within the vortex edge region during

the AASE II flight of February 13, 1992 (see Plate 3). Therefore, combining these data with the ASHOE/MAESA data, of 35 flights at high latitudes during winter, anomalous mixing lines (and hence mixing of inner vortex air into middle latitudes) were observed on only one flight. Hence, this combined data set provides very strong evidence that, at ER-2 cruise altitudes (450-500 K), inner vortex air is rarely mixed into middle latitudes during winter in sufficient quantities to effect a measurable change in tracer concentrations there (see also, Keim *et al.*, [this issue]). Furthermore, the one exception (February 13, 1992) occurred following a large-amplitude wave event in which the polar vortex was highly distorted [e.g., Plumb *et al.*, 1994], and it is during such events that modeling and trajectory studies indicate that there can be significant exchange between the inner-vortex and middle latitudes [WMO 1995, and references therein].

As anomalous mixing lines will also appear in tracer-tracer scatter plots when there is mixing of midlatitude air into the vortex (if there is curvature in the appropriate region of the standard tracer-tracer relationship), the frequency of these lines reveals information about the mixing into the polar vortices. The lack of mixing lines in the appropriate regions of the  $\text{NO}_y\text{:N}_2\text{O}$  and  $\text{CFC-11:N}_2\text{O}$  scatterplots from AASE II implies that mixing into the inner vortex was not observed during AASE II. Unfortunately, as  $\text{CFC-11}$  and  $\text{CO}_2$  were not measured and there was large-scale denitrification during the earlier campaigns (AAOE and AASE I), we cannot draw any conclusions about mixing into the vortices from the tracer-tracer plots from these campaigns.

Mixing lines were observed in the scatterplots of  $\text{CO}_2\text{:N}_2\text{O}$  but not in the scatterplots of the other long-lived tracers for measurements from the spring deployment of ASHOE/MAESA. Together, these data therefore support the premise that during southern spring there is mixing of vortex edge, but not inner vortex, air with midlatitude air. As  $\text{CO}_2$  was not measured on the AASE I and II campaigns it is not possible to say, from tracer-tracer scatterplots, whether this mixing of edge air occurs during northern winter/spring (although trajectory studies suggest that it does [e.g., Waugh *et al.*, 1994; Dahlberg and Bowman, 1994]).

Measurements made during SPADE show anomalous mixing lines in the scatterplots of all long-lived tracers (with curvature in their interrelationships), indicating that after the breakup of the Arctic polar vortex, inner vortex air is mixed into middle latitudes. CA calculations show that after the breakup the fragments of the vortex are rapidly stretched into thin filaments (sheets) which are stirred into middle latitudes. Furthermore, comparisons of observations with calculations using a one-dimensional strain-diffusion model suggest that this exvortex air is completely mixed into middle latitudes within a month (however, there are large uncertainties in the values of the parameters, particularly the diffusion coefficient, used in this model). Note that the

above mixing following the vortex breakup is faster than in the study of Hess [1991].

As noted in the introduction, the occurrence of mixing lines when vortex air is mixed with midlatitude air is related to the breakdown of slope equilibrium near the vortex edge. Slope equilibrium also breaks down in the subtropics: there are steep tracer gradients at the subtropical edge of the surf zone [e.g., Proffitt et al., 1989b; Trepte and Hitchman, 1992; Randel et al., 1993; Grant et al., 1994; Murphy et al., 1993]. As in the case of the vortex edge, mixing lines can occur when there is transport/mixing across the "subtropical barrier". Note that these mixing lines can occur if there is mixing out of the tropics without mixing into the tropics (i.e., irrespective of whether or not the atmosphere behaves like the "tropical pipe" model of Plumb [1996]). Subtropical mixing lines can be seen in the  $\text{NO}_y/\text{O}_3$  scatterplots from several flights from AASE II and ASHOE/MAESA (e.g., flight of March 27, 1994 [Fahey et al., 1996]).

Measurements made over the next three years as part of the Stratospheric Tracers of Atmospheric Transport (STRAT) campaign should provide data that will enable further examination of the mixing across both the vortex edge and the subtropical barrier.

**Acknowledgments.** We thank R.J. Atkinson for helpful discussions and comments on the manuscript, and the entire SPADE and ASHOE/MAESA teams for their support during the course of both experiments. This work was supported by the Australian Government Cooperative Research Centres Program, NSF grant ATM-92-18841 and NASA grant NAGW-1727 to MIT, a U.S. Department of Energy Global Change Distinguished Postdoctoral Fellowship to K.A. Boering, the NASA Upper Atmosphere Research Program and the NASA High Speed Research Program.

## References

- Boering, K.A., B. C. Daube, S. C. Wofsy, M. Loewenstein, J. R. Podolske, and E. R. Keim, Tracer-tracer relationships and lower stratospheric dynamics:  $\text{CO}_2$  and  $\text{N}_2\text{O}$  correlations during SPADE, *Geophys. Res. Lett.*, **21**, 2567-2571, 1994.
- Boering, K.A., E. J. Hintsa, S. C. Wofsy, J. G. Anderson, B. C. Daube, A. E. Dessler, M. Loewenstein, M. P. McCormick, J. R. Podolske, E. M. Weinstock, and G. K. Yue, Measurements of stratospheric carbon dioxide and water vapor at northern midlatitudes: Implications for troposphere-to-stratosphere transport, *Geophys. Res. Lett.*, **22**, 2737-2740, 1995.
- Chen, P., The permeability of the Antarctic vortex edge, *J. Geophys. Res.*, **99**, 20563-20571, 1994.
- Dahlberg, S.P., and K.P. Bowman, Climatology of large-scale isentropic mixing in the Arctic winter stratosphere from analyzed winds, *J. Geophys. Res.*, **99**, 20585-20599, 1994.
- Elkins, J.W., et al., NOAA/GMCC halocarbons and nitrous oxide measurements at the south pole, *Antarct. J. U. S.*, **23**, 76-77, 1988.
- Elkins, J.W., T. M. Thompson, T. H. Swanson, J. H. Butler, B. D. Hall, S. O. Cummings, D. A. Fisher, and A. G. Raffo, Decrease in the growth rates of atmospheric chlorofluorocarbons 11 and 12, *Nature*, **364**, 780-783, 1993.
- Elkins, J.W., et al., Airborne gas chromatograph for in situ measurements of long-lived species in the upper troposphere and lower stratosphere, *Geophys. Res. Lett.*, **23**, 347-350, 1996.
- Emanuel, K. A., *Atmospheric Convection*, Oxford Univ. Press, New York, 1994.
- Fahey, D.W., D. M. Murphy, K. K. Kelly, M. K. W. Ko, M. H. Proffitt, C. S. Eubank, G. V. Ferry, M. Loewenstein, and K. R. Chan, Measurements of nitric oxide and total reactive nitrogen in the Antarctic stratosphere: Observations and chemical implications, *J. Geophys. Res.*, **94**, 16,665-16,682, 1989.
- Fahey, D.W., K. K. Kelly, S. R. Kawa, A. F. Tuck, M. Loewenstein, K. R. Chan, and L. E. Heidt, Observations of denitrification and dehydration in the winter polar stratospheres, *Nature*, **344**, 321-324, 1990a.
- Fahey, D.W., S. Solomon, S. R. Kawa, M. Loewenstein, J.R. Podolske, S.E. Strahan, and K. R. Chan, A diagnostic for denitrification in the winter polar stratospheres, *Nature*, **345**, 698-702, 1990b.
- Fahey, D.W., et al., In situ observations of  $\text{NO}_y$ ,  $\text{O}_3$ , and the  $\text{NO}_y/\text{O}_3$  ratio in the lower stratosphere, *Geophys. Res. Lett.*, **23**, 1653-1656, 1996.
- Grant, W. B., E.V. Browell, J. Fishman, V.G. Brackett, R.E. Veiga, D. Nganga, A. Minga, B. Cross, C. Butler, M. Fenn, C.S. Long, and L.L. Stowe, Aerosol associated changes in the tropical stratospheric ozone following the eruption of Mount Pinatubo, *J. Geophys. Res.*, **99**, 8197-8211, 1994.
- Hall, T.M., and M.J. Prather, Seasonal evolutions of  $\text{N}_2\text{O}$ ,  $\text{O}_3$ , and  $\text{CO}_2$ : Three-dimensional simulations of stratospheric correlations, *J. Geophys. Res.*, **100**, 16699-16720, 1995.
- Hartmann, D.L., L.E. Heidt, M. Loewenstein, J.R. Podolske, J. Vedder, W.L. Starr, and S.E. Strahan, Transport into the south polar vortex in early spring, *J. Geophys. Res.*, **94**, 16779-16796, 1989.
- Hess, P.G., Mixing processes following the final stratospheric warming, *J. Atmos. Sci.*, **48**, 1625-1641, 1991.
- Kawa, S.R., R.A. Plumb and U. Schmidt, Correlations of long-lived species in simultaneous observations, In *The Atmospheric Effects of Stratospheric Aircraft: Report of the 1992 Models and Measurements Workshop*, edited by M.J. Prather and E.E. Remsburg, 1993.
- Keim, E.R., et al., Measurements of the  $\text{NO}_y/\text{N}_2\text{O}$  correlation in the lower stratosphere: Latitudinal and seasonal changes and model comparisons, *J. Geophys. Res.*, this issue.
- Kelly, K.K., et al., Dehydration in the lower Antarctic stratosphere during late winter and early spring, *J. Geophys. Res.*, **94**, 11,317-11,357, 1989.
- Loewenstein, M., J.R. Podolske, and S.E. Strahan, ATLAS instrument characterization: Accuracy of the AASE and AAOE nitrous oxide data sets, *Geophys. Res. Lett.*, **17**, 481-484, 1990.
- Loewenstein, M., J.R. Podolske, D.W. Fahey, E.L. Woodbridge, P. Tin, A. Weaver, P.A. Newman, S.E. Strahan, S.R. Kawa, M.R. Schoeberl, and L.R. Lait, New observations of the  $\text{NO}_y/\text{N}_2\text{O}$  correlation in the lower stratosphere, *Geophys. Res. Lett.*, **20**, 2531-2534, 1993.
- Manney, G., et al., Chemical depletion of lower stratospheric ozone in the 1992-1993 northern winter vortex, *Nature*, **370**, 429-434, 1994a.
- Manney, G., R. W. Zurek, M. Gelman, A. Miller, and R. Nagatani, The anomalous Arctic lower stratospheric polar vortex of 1992-1992, *Geophys. Res. Lett.*, **21**, 2405-2409, 1994b.
- Murphy, D. M., and D. W. Fahey, An estimate of the flux of stratospheric reactive nitrogen and ozone into the troposphere, *J. Geophys. Res.*, **99**, 5325-5332, 1994.
- Murphy, D. M., D. W. Fahey, M. H. Proffitt, S. C. Liu,

- K. R. Chan, C. S. Eubank, S. R. Kawa, K. K. Kelly, Reactive nitrogen and its correlation with ozone in the lower stratosphere and upper troposphere, *J. Geophys. Res.*, **98**, 8751-8773, 1993.
- Nash, E.R., P.A. Newman, J.E. Rosenfield, and M.R. Schoeberl, An objective determination of the polar vortex using Ertel's potential vorticity, *J. Geophys. Res.*, **101**, 9471-9478, 1996.
- Newman, P.A., et al., Measurements of polar vortex air in the midlatitudes, *J. Geophys. Res.*, **101**, 12,879-12,893, 1996.
- Norton, W. A., Breaking Rossby waves in a model stratosphere diagnosed by a vortex-following coordinate system and a contour advection technique, *J. Atmos. Sci.*, **51**, 654-673, 1994.
- Pierce, B.R., and T.D.A. Fairlie, Chaotic advection in the stratosphere: Implications for the dispersal of chemically perturbed air from the polar vortex, *J. Geophys. Res.*, **98**, 18589-18595, 1993.
- Plumb, R.A., A tropical pipe model of stratospheric transport, *J. Geophys. Res.*, **101**, 3957-3972, 1996.
- Plumb, R.A., and M.K.W. Ko, Interrelationships between mixing ratios of long-lived stratospheric constituents, *J. Geophys. Res.*, **97**, 10145-10156, 1992.
- Plumb, R.A., D.W. Waugh, R.J. Atkinson, M.R. Schoeberl, L.R. Lait, P.A. Newman, E.V. Browell, A. Simmons, and M. Loewenstein, Intrusions into the lower stratospheric Arctic vortex during the winter of 1991/92, *J. Geophys. Res.*, **99**, 1089-1106, 1994.
- Prather, M., and A.H. Jaffe, Global impact of the Antarctic ozone hole: Chemical propagation, *J. Geophys. Res.*, **95**, 3473-3492, 1990.
- Proffitt, M.H., D.W. Fahey, K.K. Kelly, and A.F. Tuck, High latitude ozone loss outside the Antarctic ozone hole, *Nature*, **342**, 233-237, 1989a.
- Proffitt, M.H., K.K. Kelly, J.A. Powell, B. Gary, M. Loewenstein, J.R. Podolske, J. Vedder, W.L. Starr, and S.E. Strahan, Evidence for diabatic cooling and poleward transport within and around 1987 Antarctic ozone hole, *J. Geophys. Res.*, **94**, 16797-16813, 1989b.
- Proffitt, M.H., M.J. Steinkamp, J.A. Powell, R. McLaughlin, O.A. Mills, A.L. Schmeltekopf, T.L. Thompson, A.F. Tuck, T. Tyler, R. H. Winkler, and K.R. Chan, In situ ozone measurements within the 1987 Antarctic ozone hole from a high-altitude ER-2 aircraft, *J. Geophys. Res.*, **94**, 16547-16556, 1989c.
- Proffitt, M.H., J. Margitan, K. Kelly, M. Loewenstein, J. Podolske, and K. Chan, Ozone loss in the Arctic polar vortex inferred from high altitude aircraft measurements, *Nature*, **342**, 31-36, 1990.
- Proffitt, M.H., K. Aikin, J. Margitan, M. Loewenstein, J. Podolske, A. Weaver, K.R. Chan, H. Fast, and J.W. Elkins, Ozone loss inside the northern polar vortex during the 1991-92 winter, *Science*, **261**, 1150-1154, 1993.
- Randel, W.J., Ideas flow on Antarctic vortex, *Nature*, **364**, 105-106, 1993.
- Randel, W.J., J.C. Gille, A.E. Roche, J.B. Kumer, J.L. Mergenthaler, J.W. Waters, E.F. Fishbein, and W.A. Lahoz, Planetary wave mixing in the subtropical stratosphere observed in UARS constituent data, *Nature*, **365**, 533-535, 1993.
- Schubert, S.D., R.B. Rood, and J. Pfandner, An assimilated data set for Earth science applications, *Bull. Am. Meteorol. Soc.*, **74**, 2331-2342, 1993.
- Strahan, S. E., and J. D. Mahlman, Evaluation of the SKYHI general circulation model using aircraft N<sub>2</sub>O measurements: 1. Polar winter stratospheric meteorology and tracer morphology, *J. Geophys. Res.*, **99**, 10,305-10,318, 1994.
- Swinbank, R., and A. O'Neill, A stratosphere-troposphere data assimilation system, *Mon. Weather Rev.*, **122**, 686-702, 1994.
- Trepte, C.R. and M.H. Hitchman, Tropical stratospheric circulation deduced from satellite aerosol data, *Nature*, **355**, 626-628, 1992.
- Tuck, A.F., D. W. Fahey, M. Loewenstein, J.R. Podolske, K.K. Kelly, S.J. Hovde, D.M. Murphy, and J. W. Elkins, Spread of denitrification from 1987 Antarctic and 1988-1989 Arctic stratospheric vortices, *J. Geophys. Res.*, **99**, 20,573-20,583, 1994.
- Volk, C.M., J. W. Elkins, D. W. Fahey, R. J. Salawitch, G. S. Dutton, J. M. Gilligan, M. H. Proffitt, M. Loewenstein, and P. R. Podolske, In situ measurements constraining exchange between the tropics and middle latitudes in the lower stratosphere, *Science*, **272**, 1763-1768, 1996.
- Waugh, D.W., and R.A. Plumb, Contour advection with surgery: A technique for investigating fine scale structure in tracer transport, *J. Atmos. Sci.*, **51**, 530-540, 1994.
- Waugh, D.W., R.A. Plumb, R.J. Atkinson, M.R. Schoeberl, L.R. Lait, P.A. Newman, M. Loewenstein, D.W. Toohey, and C.R. Webster, Transport of material out of the stratospheric Arctic vortex by Rossby wave breaking, *J. Geophys. Res.*, **99**, 1071-1088, 1994.
- Wofsy, S.C., R. Cohen, and A. Schmeltekopf, Overview: The Stratospheric Photochemistry Aerosols and Dynamics Expedition (SPADE) and Airborne Arctic Stratospheric Expedition II (AASE II), *Geophys. Res. Lett.*, **21**, 2535-2539, 1994a.
- Wofsy, S.C., K.A. Boering, B.C. Daube, and M.B. McElroy, Vertical transport rates in the stratosphere in 1993 from observations of CO<sub>2</sub>, N<sub>2</sub>O, and CH<sub>4</sub>, *Geophys. Res. Lett.*, **21**, 2571-2574, 1994b.
- Woodbridge, E.L., et al., Estimates of total organic and inorganic chlorine in the lower stratosphere from in situ and flask measurements, *J. Geophys. Res.*, **100**, 3057-3064, 1995.
- World Meteorological Organization (WMO), *Scientific Assessment of Ozone Depletion: 1994*, 451 pp., Geneva, 1995.

K.A. Boering, B.C. Daube, S.C. Wofsy, Department of Earth and Planetary Sciences, Harvard University, Cambridge, MA 02138. (e-mail: kab@io.harvard.edu; bcd@io.harvard.edu; scw@io.harvard.edu)

K. R. Chan, M. Loewenstein, J. R. Podolske, NASA Ames Research Center, Moffett Field, CA 94035-1000. (e-mail: roland\_chan@qmgate.arc.nasa.gov; loewen@argus.arc.nasa.gov; podolske@argus.arc.nasa.gov)

G. S. Dutton, J. W. Elkins, C. M. Volk, NOAA Climate Monitoring and Diagnostics Laboratory, Boulder, CO 80303 (e-mail: gdutton@cmdl.noaa.gov; jelkins@cmdl.noaa.gov; mvolk@cmdl.noaa.gov)

D. W. Fahey, M. H. Proffitt, K. K. Kelly, NOAA Aeronomy Laboratory, Boulder, CO 80303 (e-mail: fahey@al.noaa.gov; kellyk@al.noaa.gov; proffitt@al.noaa.gov)

R.-S. Gao, E. Keim, Cooperative Institute for Research in Environmental Science, 325 Broadway, Boulder CO 80303 (e-mail: gao@al.noaa.gov)

L. R. Lait, P. A. Newman, NASA Goddard Space Flight Center, Greenbelt, MD (e-mail: irlait@ertel.gsfc.nasa.gov; newman@notus.gsfc.nasa.gov)

R. A. Plumb, Massachusetts Institute of Technology, Cambridge, MA 02139 (e-mail: rap@rossby.mit.edu)

D. W. Waugh, Cooperative Research Centre for Southern Hemisphere Meteorology, Monash University, Wellington Rd, Clayton, Vic 3168, Australia (e-mail: vortex.shm.monash.edu.au)

(Received October 4, 1995; revised November 14, 1996; accepted December 18, 1996.)